Long-period modulated structure and electric-field-induced structural transformation in $Na_{0.5}Bi_{0.5}TiO_3$-based lead-free piezoelectrics

Dipak Kumar Khatua,[1] Anatoliy Senyshyn,[2] and Rajeev Ranjan[1,*]

[1]*Department of Materials Engineering, Indian Institute of Science, Bangalore-560012, India*

[2]*Forschungsneutronenquelle Heinz Maier-Leibnitz (FRM II). Technische Universität München, Lichtenbergestrasse 1, D-85747 Garching b. München, Germany*

(Received 28 August 2015; revised manuscript received 28 February 2016; published 14 April 2016)

$Na_{0.5}Bi_{0.5}TiO_3$- based lead-free piezoelectrics exhibiting giant piezostrain are technologically interesting materials for actuator applications. The lack of clarity with regard to the structure of the nonpolar phase of this system has hindered the understanding of the structural mechanism associated with the giant piezostrain and other related phenomena. In this paper, we have investigated the structure and field-induced phase transformation behavior of a model system $(0.94-x)Na_{0.5}Bi_{0.5}TiO_3$-$0.06BaTiO_3$-$xK_{0.5}Na_{0.5}NbO_3$ $(0.0 \leqslant x \leqslant 0.025)$. A detailed structural analysis using neutron powder diffraction revealed that the nonpolar phase is neither cubic nor a mixture of rhombohedral ($R3c$) and tetragonal ($P4bm$) phases as commonly reported in literature but exhibits a long-period modulated structure, which is most probably of the type $\sqrt{2} \times \sqrt{2} \times n$ with $n = 16$. Our results suggest that the giant piezoelectric strain is associated with a field-induced phase transformation of the long-period modulated structure to rhombohedral $R3c$ structure above a critical field. We also demonstrate that the giant piezostrain is lost if the system retains a fraction of the field-induced $R3c$ phase. A possible correlation among depolarization temperature, giant piezostrain, and its electrical fatigue behavior has also been indicated.

DOI: 10.1103/PhysRevB.93.134106

I. INTRODUCTION

Environmental concerns have led to a great surge in research interest in lead-free piezoelectric materials [1–4]. $Na_{0.5}Bi_{0.5}TiO_3$- (NBT-) based lead-free piezoelectrics are among the most extensively investigated systems in this regard [5–13]. Zhang *et al.* first reported a giant piezostrain of 0.4%−0.5% in an NBT-based system, making these materials very important from the viewpoint of actuator applications [13]. However, the understanding of the mechanism associated with this interesting phenomenon is far from complete. One of the factors which hinders this understanding is the lack of clarity with regard to the crystal structures of the NBT-based systems. NBT is known to exhibit intrinsic structural inhomogeneity which has a profound impact on the global structure, dielectric, ferroelectric, and piezoelectric behaviors [14]. Based on an x-ray diffuse scattering study, Kreisel *et al.* suggested that the Na/Bi cations in NBT are locally displaced away from the polar [111] rhombohedral direction [15]. Electron microscopy studies, on the other hand, revealed the presence of local in-phase ($a^0a^0c^+$) octahedral tilt [5,16], which is characteristic of the intermediate high-temperature (above 300 °C) $P4bm$ phase of NBT [17] in the rhombohedral ferroelectric matrix. Balagorov *et al.* reported an existence of long-period modulation in the rhombohedral phase along the [001] direction of the $P4bm$ phase [18]. Gorfmann and Thomas [19] and Aksel *et al.* [20] have questioned the conventional global rhombohedral ($R3c$) structure of NBT and suggested a monoclinic (Cc) structure. A strong correlation between the structural inhomogeneity on the local scale and the appearance of global monoclinic Cc distortion was recently demonstrated by Rao *et al.* [14]. The authors showed that a strong electric field significantly reduces the degree of structural inhomogeneity and makes the global structure appear rhombohedral ($R3c$) [21,22]. The complex structural state of NBT and its chemically modified variants are highly sensitive to slight variation in the synthesis conditions [5], mechanical stress [6], and electric field [11,19–23]. Ma *et al.* reported a change in the nature of the field-induced phase transition in 3 mol % of Ba-modified NBT [11], which was further confirmed in a detailed x-ray diffraction (XRD) and neutron-diffraction study by Rao *et al.* [24]. Ranjan and Dviwedi have reported a cubiclike structure and relaxor ferroelectric behavior in a 6-mol % Ba-modified NBT $Na_{0.5}Bi_{0.5}TiO_3$-$BaTiO_3$ (NBT-BT) [25].

The phenomenon of giant piezostrain in NBT-based systems has caught the attention of the scientific community in recent years [13,26–29]. First reported by Zhang *et al.* in a $(K_{0.5}Na_{0.5})NbO_3$- (KNN-) modified NBT-BT [13], this system has been extensively investigated over the years [30–47]. The giant piezostrian behavior has also been reported for other types of chemical modifications of NBT. For instance, Malik *et al.* [27] reported ∼0.44% piezostrain for Nb-, Sr-, and K-modified NBT. For a similar kind of chemical modification, Liu and Tan have reported a piezostrain value of 0.7% [48]. Cheng *et al.* [29] have reported a giant unipolar piezostrain of 0.42% in Ba-, Fe-, and Nb-modified NBT. A strain value of 0.48% has been reportred by Maurya *et al.* in a $K_{0.5}Bi_{0.5}TiO_3$-modified NBT-BT [49]. For a better comprehension of the mechanism associated with the giant piezostrain and related effects, it is important to understand the subtle structural features in the zero-field state and the nature of the field-induced phase transformation. Zhang and co-workers attributed the giant strain to field-induced antiferroelectric-ferroelectric phase transition [30,33]. Jo *et al.* [31], Kling *et al.* [34], and Hinterstein *et al.* [35] suggested that the transformation is from a nonpolar to a ferroelectric ($R3c$) phase. The structural state of the nonpolar phase has remained

*rajeev@materials.iisc.ernet.in

an enigma so far. Whereas x-ray-diffraction studies suggest a cubic structure [13,25] of these compositions, Schmitt *et al.* [42] have reported the coexistence of tetragonal ($P4bm$) and rhombohedral ($R3c$) phases. The idea of $R3c + P4bm$ seems to be primarily guided by the observation of $\frac{1}{2}\{ooe\}$ and $\frac{1}{2}\{ooo\}$ superlattice reflections in the diffraction patterns, where o and e represent odd and even integers, respectively. The $\frac{1}{2}\{ooe\}$ superlattice reflections are generally attributed to the $a^0a^0c^+$ octahedral tilt and the $P4bm$ phase. The $\frac{1}{2}\{ooo\}$ superlattice reflections in NBT-based systems are generally attributed to an $a^-a^-a^-$ octahedral tilt corresponding to the $R3c$ structure. A perusal of the Rietveld fitted neutron-diffraction pattern shown by Schmidt *et al.* (Fig. 1(b) in Ref. [42]) clearly suggests that the calculated position of the $\frac{1}{2}\{530\}_c$ superlattice peak is shifted from the observed superlattice reflection. This mismatch in the peak positions is a crucial indicator that the true structure need not be $P4bm$. In this paper, we have confirmed this to be the case. We have examined the structural details associated with the nonpolar phase of the model system $(0.94-x)Na_{0.5}Bi_{0.5}TiO_3$-$0.06BaTiO_3$-$xK_{0.5}Na_{0.5}NbO_3$ ($0.0 \leqslant x \leqslant 0.025$) and the phase transformation behavior on application of the electric field and temperature using an x-ray and neutron powder diffraction (NPD) study. Detailed analysis of the neutron powder diffraction of the nonpolar phase revealed that the conventional $R3c + P4bm$ two-phase model is not suitable to explain the subtle features of the neutron-diffraction pattern. We argue that the structure of the nonpolar phase consists of a long-period modulation, most probably of the type $\sqrt{2} \times \sqrt{2} \times n$ with $n = 16$. Our results show that the giant piezostrain is associated with field-induced transformation of the long-period modulated structure to the rhombohedral ($R3c$) phase. We also show that, in the scenario as the transformed $R3c$ phase is partly retained, the giant piezostrain is lost.

II. EXPERIMENT

Different compositions of $(0.94-x)Na_{0.5}Bi_{0.5}TiO_3$-$0.06BaTiO_3$-$xK_{0.5}Na_{0.5}NbO_3$ ($0 \leqslant x \leqslant 0.025$) were prepared following conventional solid-state route by mixing stoichiometric ratios of dried Na_2CO_3 [99.9%, Siesco Research Laboratory (SRL), India], Bi_2O_3 (>99%, SRL, India), TiO_2 (99.8%, Alfa Aesar), K_2CO_3 (99.5%, SRL, India), $BaCO_3$ (99.5%, Alfa Aesar), and Nb_2O_5 (99.95%, Alfa Aesar) in an acetone medium using zirconia vials and balls in a planetary ball mill for 12 h. Calcination was carried out at 900 °C for 3 h. After thorough ball milling, the calcined powder was recalcined at 900 °C for 2 h. Green pellets were made first by applying uniaxial pressure of 100 MPa and then subjecting them to cold isostatic pressing at 300 MPa. Sintering was carried out at 1150 °C for 3 h. Density measurement of the sintered pellets, using the Archimedes method, showed the pellets to be ∼95% dense. Electric poling was carried on the sintered pellets with diameters of ∼10−12 mm and thicknesses of 1–1.4 mm by applying a dc field in the range of 45–50 kV/cm for 30 min. X-ray powder diffraction (XRPD) was carried out with Cu $K\alpha_1$ radiation using a Rigaku Smartlab x-ray diffractometer. An *in situ* electric-field-dependent XRD study was carried out on the pellets. The face of the pellet facing the XRD beam was sputter coated with a thin layer of Au for application of the electric field. NPD patterns were collected at FRM-II, Germany (wavelength of 1.5483 Å). Powders for XRD and NPD were prepared after gentle crushing of as sintered and poled pellets. Dielectric measurements were carried out on a Novocontrol impedance analyzer (Alpha-A). A precision Premier II tester (Radiant Technology, Inc.) was used for the electric-field-polarization (E-P) measurement. A direct piezoelectric coefficient d_{33} was measured using Piezotest, PM300. An electric-field-dependent strain measurement was performed using a MTI-2100 FOTONIC sensor attached to the Radiant setup. Structural analysis was carried out by the Rietveld method using the FULLPROF package [50].

III. RESULTS

A. Dielectric, ferroelectric, and piezoelectric responses

Figure 1 shows the polarization and strain response as a function of compositions under different unipolar and bipolar electric fields. For $x = 0$, the shape of the P-E loop is similar to that of a normal ferroelectric [Fig. 1(a)]. For $x = 0.01$ (0.01 KNN), two anomalies develop: (i) a sudden jump in polarization and (ii) significant constriction of the loop in the middle. This composition also exhibits the giant piezostrain by way of an abrupt increase in the strain value in the field range of 35–45 kV/cm both in the bipolar and in the unipolar cycles, shown in Figs. 1(b) and 1(d),respectively. The maximum strain we obtained was 0.3% at 45 kV/cm. However, during the subsequent cycles the maximum strain was found to decrease even while the amplitude of the field was increased beyond the value in the previous [Fig. 2(a)] cycle. This fatigue effect is in conformity with what was earlier reported by Luo *et al.* [51]. In a separate experiment, we poled the specimen at 45 kV/cm for 30 min and carried out the strain-field measurements. This specimen exhibited a significantly reduced strain of 0.13% at 50 kV/cm [Fig 2(a)]. The original giant strain could however be recovered after

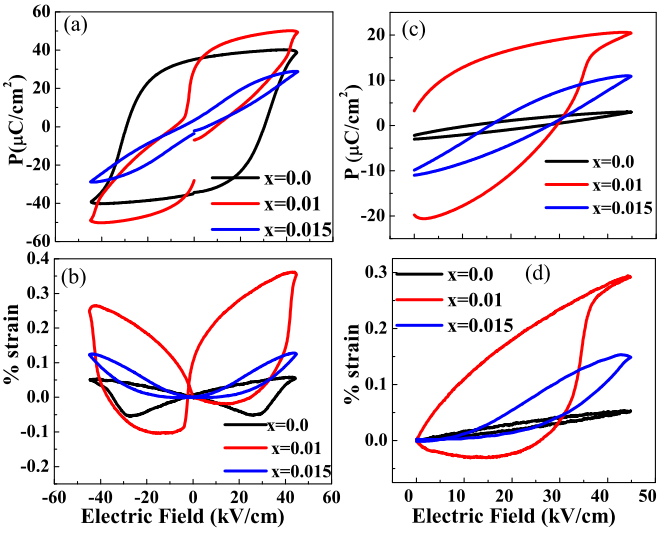

FIG. 1. Electric-field-dependent polarization and strain measurement for different $(0.94-x)$NBT-0.06BT-x KNN compositions at an electric field of 45 kV/cm. (a) Bipolar P-E, (b) bipolar S-E, (c) unipolar P-E, and (d) unipolar S-E.

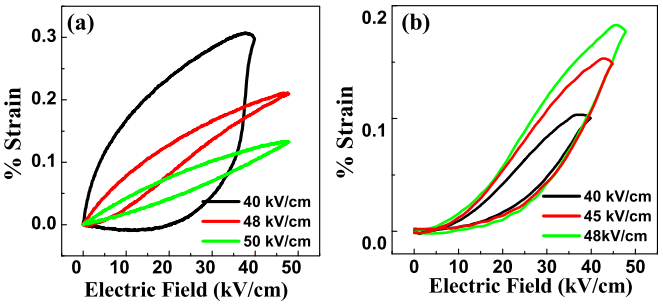

FIG. 2. Electric-field-dependent unipolar strain of (a) 0.01 KNN and (b) 0.015 KNN. The amplitude of the field was increased in subsequent cycles. In (a) the strain loop with the green color has taken on a sample poled at 45 kV/cm for 30 min.

heating the poled specimen at 100 °C. Figure 3 shows the temperature-dependent dielectric measurement on a poled specimen of $x = 0.01$ during heating and cooling cycles. The important point to note is the occurrence of a weak but sharp dielectric anomaly at $T_d = 60$ °C during the heating cycle and its disappearance during the cooling cycle. In analogy with a similar observation in (NBT) [14] and NBT-BT [10], the weak but sharp anomaly in the heating cycle of the poled specimen suggests that poling stabilized a noticeable fraction of the ferroelectric phase, which depolarizes at T_d on heating. The recovery of the giant strain after heating the poled specimen at 100 °C is therefore associated with the dissolving of the field-induced ferroelectric phase and restoring the nonpolar relaxor state.

The inducement of the irreversible ferroelectric phase after subjecting the specimen $x = 0.01$ to a strong electric field was separately verified by measuring the weak signal longitudinal

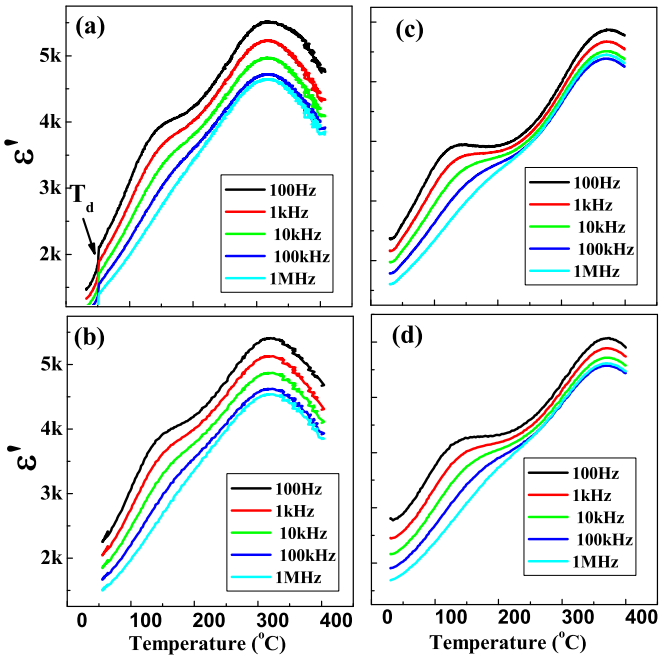

FIG. 3. Temperature-dependent permittivity of $(0.94 - x)$NBT-0.06BT-x KNN with (a) 0.01 KNN poled, (b) 0.01 KNN unpoled, (c) 0.015 KNN poled, and (d) 0.015 KNN unpoled.

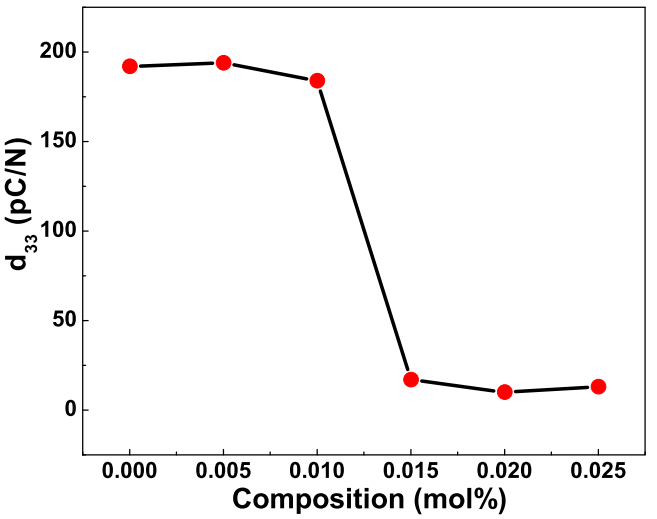

FIG. 4. Composition dependence of longitudinal piezoelectric coefficient (d_{33}) for $(0.94 - x)$NBT-0.06BT-x KNN. Samples were poled at 45 kV/cm for 0.5 h.

direct piezoelectric response (d_{33}) on poled specimens using a Berlincourt-based piezometer. Evidently, only those specimens would show a measurable direct piezoelectic d_{33} signal

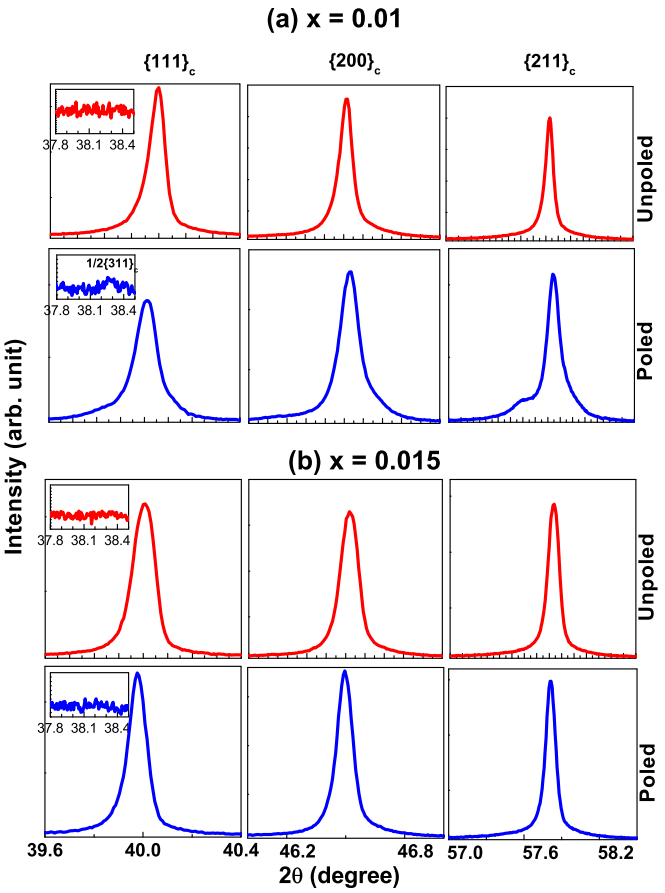

FIG. 5. Comparison of unpoled and poled XRD patterns of selected Bragg reflections of $(0.94 - x)$NBT-0.06BT-x KNN. Poled specimens show peak splitting irreversibly for the composition range of $0.0 \leqslant x \leqslant 0.01$. The insets show the position of the $\frac{1}{2}\{311\}_c$ superlattice reflection which becomes after poling $x = 0.01$.

which would stabilize the ferroelectric phase after poling. As shown in Fig. 4, d_{33} remains nearly constant (~190 pC/N) in the composition range of $0 \leqslant x \leqslant 0.01$ and drops sharply to zero for $x > 0.01$. This implies that the compositions $x > 0.01$ could not be poled up even on application of a field of about 50 kV/cm. This was the limiting field in our case since the specimens were undergoing frequent electric breakdown for fields above 50 kV/cm. Consistent with the absence of the d_{33} signal for $x > 0.01$, the poled specimens of $x > 0.01$ do not exhibit any sharp dielectric anomaly corresponding to thermal depolarization [Fig. 3(c)]. Unlike with $x = 0.01$, the compositions $x > 0.01$ did not show an abrupt increase in the piezostrain above a critical field. For example, for $x = 0.015$ (0.015 KNN) the strain at 40 kV/cm is 0.12%, which is nearly half the value obtained from $x = 0.01$ at the same field [Fig. 1(b)]. However, most significantly, unlike $x = 0.01, x = 0.015$ does not show a decrease in the high-field piezostrain in the subsequent cycles. Contrary to $x = 0.01$, the strain value increased from 0.12% to 0.20% when the electric-field amplitude was increased from 40 kV/cm in the first cycle to 48 kV/cm in the third cycle [Fig. 2(b)]. Also, $x = 0.015$ did not show a decrease in the strain value after poling. Since, as shown above, the specimen exhibiting a strong decrease in giant piezostrain above the critical field also stabilizes a ferroelectric phase, it appears that the electrical fatigue in this system is of structural origin. This aspect is detailed in the following sections.

B. Insufficiency of the *P*4*bm* + *R*3*c* phase coexistence model

Figure 5 shows the XRPD patterns of $(0.94 - x)Na_{0.5}Bi_{0.5}TiO_3$-$0.06BaTiO_3$-$xK_{0.5}Na_{0.5}NbO_3$. In conformity with the earlier reports [13,25], all the Bragg peaks of these compositions are singlet in the unpoled state, suggesting a cubic structure,. The cubic lattice parameter and the volume, however, increase with increasing KNN concentration. In

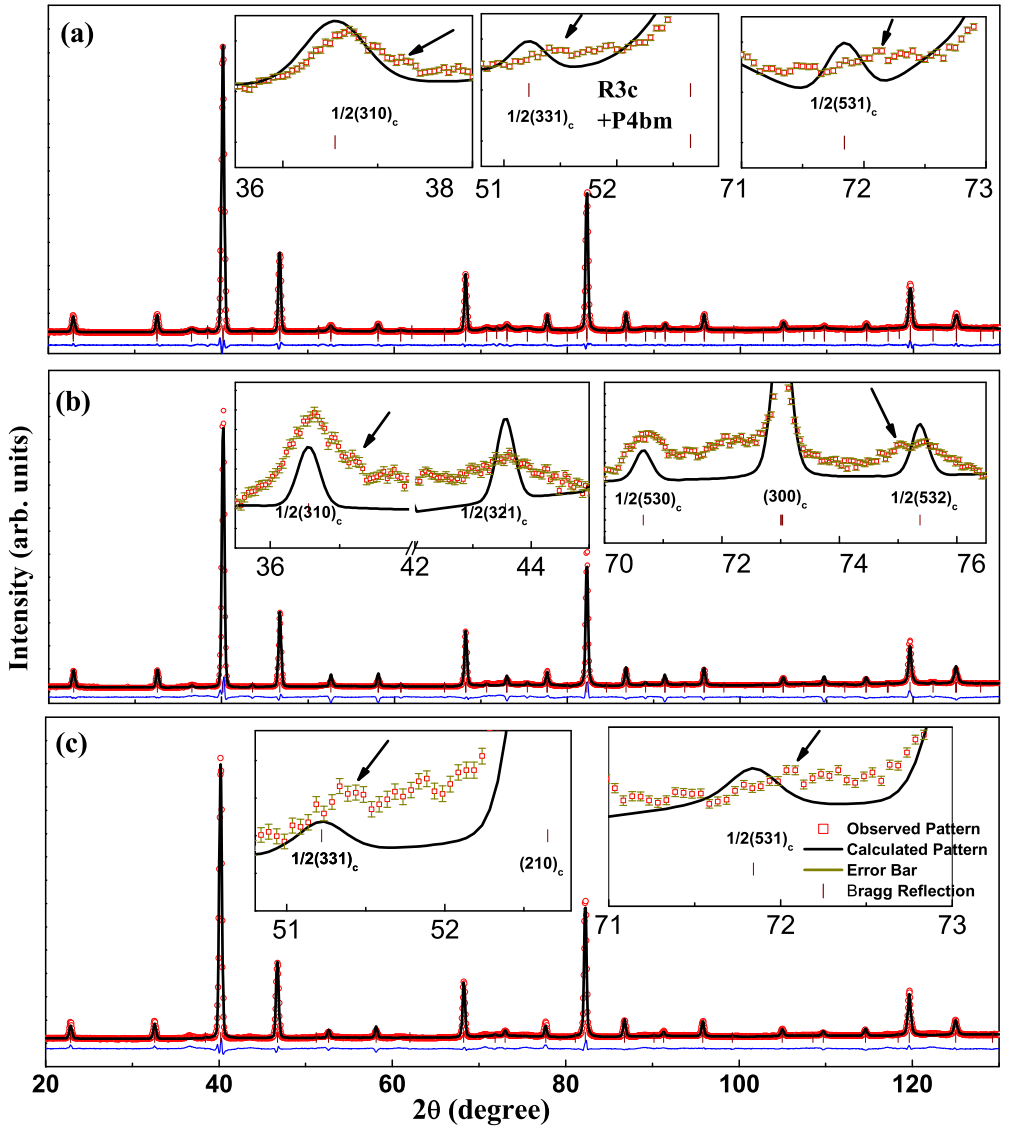

FIG. 6. (a) Le Bail fitting with $R3c + P4bm$ phase coexistence model of the neutron powder diffraction pattern of unpoled 0.01 KNN, (b) Rietveld fitting with the $P4bm$ phase, and (c) Rietveld fitting with the $R3c$ phase. The insets show the 2θ regions exhibiting the misfit between the observed and the calculated superlattice reflections. The error bars are shown for each data point.

contrast to the XRPD patterns, the NPD patterns of all the unpoled compositions show weak superlattice reflections. This implies that the true structure of NBT-BT-KNN in the unpoled state must be noncubic albeit a cubic metric. In the past, the structure of these compositions has been reported to be a coexistence of $P4bm$ and $R3c$ [39,42]. However, our attempt to fit the NPD data with the $P4bm + R3c$ model turned out to be highly unsatisfactory [Fig. 6(a)]. We noted that the refinement was nonconverging (oscillating R factors). The oscillatory refinement is primarily due to the fact that both, $P4bm$ and $R3c$, had to fit exactly the same set of main Bragg profiles. In such a scenario, there is no way to establish a unique ratio of the coexisting $R3c$ and $P4bm$ phases. This led to arbitrary variations in the scale factors of the $P4bm$ and the $R3c$ phases. Furthermore, even though the $P4bm$ and $R3c$ symmetries allow independent refinement of the two lattice parameters of these phases, their refinement also led to nonconvergence of the fit. This is because even a slight change in the lattice parameters would lead to distortion of the cubic metric, which was not acceptable since the all the Bragg peaks are singlet in nature, suggesting a cubic lattice. In the next step we attempted to fit the NPD with one phase at a time to account for the weak superlattice reflections. Earlier, Schmidt *et al.* [42] and Hinterstein *et al.* [35] have argued about the plausibility of the $P4bm$ structure in their neutron-diffraction study by highlighting the fit of the $\frac{1}{2}\{530\}_c$ and $\frac{1}{2}\{532\}_c$ superlattice reflections. A careful observation of the fit shown by these authors, however, suggests a misfit in the positions of the observed and calculated $\frac{1}{2}\{530\}_c$ peak. It may, however, be noted that the $P4bm$ model also predicts prominent superlattice reflections with pseudocubic index $\frac{1}{2}\{310\}_c$ and $\frac{1}{2}\{312\}_c$ at lower angles. In our NPD pattern these superlattice reflections are expected to appear at $2\theta \sim 36.5^\circ$ and $\sim 43.5^\circ$, respectively. As per the $P4bm$ model, the intensity of the calculated superlattice peak $\frac{1}{2}\{312\}_c$ at $2\theta = 43.5^\circ$ is expected to be higher than the intensity of the calculated superlattice peak $\frac{1}{2}\{310\}_c$ at 36.5°. In contrast, the observed intensities show the opposite trend. More importantly, whereas the $P4bm$ model predicts only one peak at $2\theta = 36.5^\circ$, the observed profile suggests additional superlattice reflections on either side of this peak [the inset of Fig. 6(b)]. Similarly, a careful observation reveals the occurrence of rwo closely spaced peaks near the $\frac{1}{2}\{532\}_c$ position. We also attempted to fit the superlattice peaks observed at positions close to that anticipated by the $R3c$ model. This too was found to be unsatisfactory as demonstrated in the insets of Fig. 6(c). For example, the $R3c$ model predicts a superlattice peak at 51.23°, whereas the observed peak is at 51.39°. Similarly the $R3c$ model predicts a superlattice peak at 71.84° whereas the

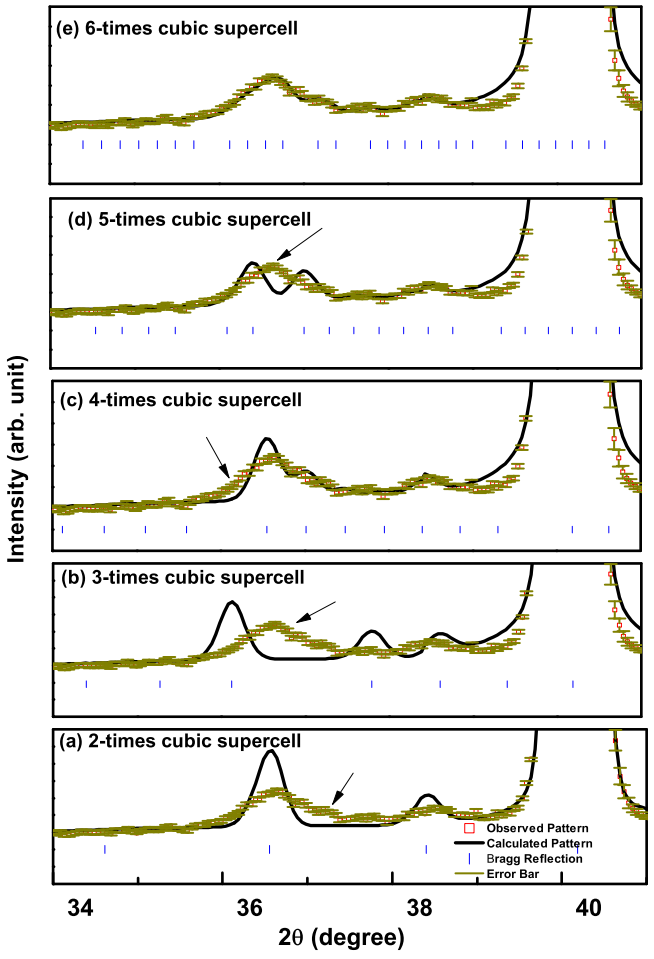

FIG. 7. Le Bail fitting of the neutron powder diffraction pattern of unpoled 0.01 KNN with (a) $2 \times 2 \times 2$-, (b) $3 \times 3 \times 3$-, (c) $4 \times 4 \times 4$-, (d) $5 \times 5 \times 5$-, and (e) $6 \times 6 \times 6$-type cubic supercells. The arrows highlight the misfit regions. The error bars for each data point are shown.

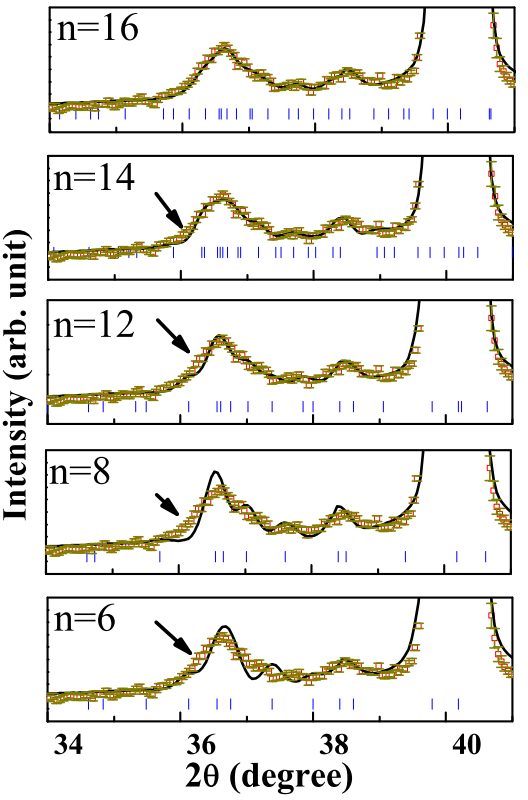

FIG. 8. Le Bail fitting of the neutron powder diffraction pattern of unpoled 0.01 KNN fitted with a $\sqrt{2}a \times \sqrt{2}b \times nc$-type cell with $n = 6$, $n = 8$, $n = 12$, $n = 14$, and $n = 16$. The arrows highlight the misfit regions. The error bars for each data point are shown.

observed peak is located at 72.13°. Since in all the fittings the fundamental Bragg peak positions were exactly matched, the slight difference between the observed and the calculated peak positions of the superlattice reflections assumes great significance. Schmidt *et al.*, perhaps, did not see the existence of superlattice peaks in very close proximity and interpreted it as considerable broadening of the superlattice reflections due to the $P4bm$ and $R3c$ phases [42]. Accordingly, the authors argued about the existence of octahedral tilts of short coherence length as compared to the coherence of the pseudocubic matrix [42]. Since Rietveld refinement cannot simultaneously account for the extraordinarily different widths of the fundamental and the superlattice reflections, a pair distribution function analysis of the total scattering data would be more appropriate to obtain the complex structural information. The recognition of more than one superlattice reflection in close proximity, however, offers a way to address the average crystal structure via a supercell approach. By predicting additional reflections, the supercell can, in principle, account for multiple superlattice reflections in close proximity without the need to invoke two different coherence lengths for the superlattice and the fundamental reflections. At the same time, in the absence of a noncubic splitting in the fundamental Bragg peaks, it is necessary for the supercell to possess a cubic metric.

C. Evidence of a long-period structural modulation in the nonpolar state

Our approach to obtain a suitable structural model for the nonpolar phase is based on the identification of the smallest size supercell which can index all the superlattice reflections in the neutron powder diffraction pattern by Le Bail fitting

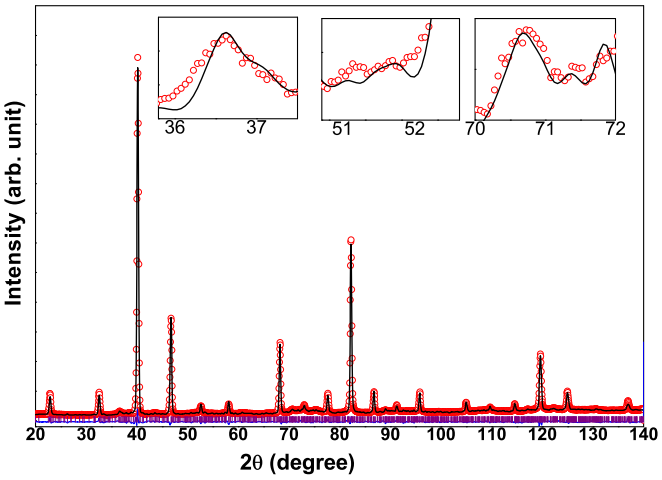

FIG. 9. The Rietveld fitted neutron powder diffraction pattern of unpoled 0.01 KNN with the long-period modulated structure (see the text). The inset shows those regions where the superlattice peaks were not accurately accounted by the $R3c$ and $P4bm$ phases.

[52]. We first attempted to index the superlattice peaks by considering equal modulation of the cubic cell on all sides, i.e., a supercell of the type $n\boldsymbol{a} \times n\boldsymbol{b} \times n\boldsymbol{c}$. The result of fitting with a doubled cubic cell ($n = 2$) is shown in Fig. 7(a). Similar to the $P4bm + R3c$ model discussed in the previous section, the $2 \times 2 \times 2$ supercell fails to index accurately all the superlattice peaks. This rules out any plausible structural model based on the simple octahedral tilt systems suggested by Glazer [53] since the maximum supercell size for plausible structural

TABLE I. Refined structural parameters from the NPD pattern for unpoled 0.01 KNN in the orthorhombic *Pbnm* space group.

Space group: *Pbnm*				
Atoms	x	y	z	B (Å^2)
$Na_1/Bi_1/Ba_1/K_1$	0.542(2)	−0.008(6)	0.033(1)	3.219(4)
$Na_2/Bi_2/Ba_2/K_2$	0.505(1)	−0.035(1)	0.095(2)	2.727(0)
$Na_3/Bi_3/Ba_3/K_3$	0.578(9)	0.018(1)	0.155(1)	1.924(6)
$Na_4/Bi_4/Ba_4/K_4$	0.483(3)	0.004(2)	0.218(3)	2.812(2)
Ti_1/Nb_1	0.000(0)	0.000(0)	0.000(0)	0.353(2)
Ti_2/Nb_2	0.010(7)	0.014(1)	0.250(0)	3.236(2)
Ti_3/Nb_3	0.002(4)	−0.007(0)	0.064(0)	2.040(2)
Ti_4/Nb_4	0.006(4)	0.002(3)	0.124(1)	1.345(9)
Ti_5/Nb_5	−0.001(3)	0.007(1)	0.187(1)	0.358(1)
O_1	−0.001(9)	−0.064(1)	0.031(1)	2.015(4)
O_2	0.235(1)	0.255(9)	0.062(1)	1.471(2)
O_3	0.725(1)	0.761(9)	0.062(1)	1.922(4)
O_4	0.271(1)	0.213(9)	0.001(1)	0.649(7)
O_5	0.012(1)	−0.043(2)	0.093(1)	2.580(9)
O_6	0.021(9)	−0.024(1)	0.155(2)	1.218(1)
O_7	0.269(0)	0.235(0)	0.124(0)	1.795(1)
O_8	0.744(0)	0.777(0)	0.123(4)	2.281(2)
O_9	0.262(4)	0.264(4)	0.186(3)	1.549(3)
O_{10}	0.739(4)	0.754(3)	0.188(3)	1.249(2)
O_{11}	−0.001(4)	−0.053(3)	0.219(0)	2.870(0)
O_{12}	0.248(6)	0.248(5)	0.250(0)	2.213(4)
O_{13}	0.764(5)	0.740(5)	0.250(0)	0.536(3)

$a = 5.5205(3)$ Å, $b = 5.5219(3)$ Å, $c = 62.4480(3)$ Å, $V = 1903.69(1)$ Å^3, R_p : 3.67, R_{wp} : 4.74R_{exp} : 1.69, and χ^2: 7.85.

models based on simple tilts is $2 \times 2 \times 2$. A need for considering higher-order structural modulation, therefore, arose. In the next step, we gradually increased the modulation period n and found $n = 6$ to be the minimum period which fitted all the superlattice peaks accurately, Fig. 7(e). This supercell cell has its volume 216 times the volume of the primitive cubic cell. We also searched for supercells with smaller volumes by allowing for nonequal modulation of the cube sides. In this context, we were primarily guided by the $\sqrt{2} \times \sqrt{2} \times n$ type of supercells reported before in (Sr,Ca)TiO_3 [54,55], $NaNbO_3$ [56], and the recent theoretical predictions by Prosandeev *et al.* in $BiFeO_3$ [57]. For $n = 1$, the supercell is similar to that of the $P4bm$ structure. The smallest n required to fit the peak positions accurately was found to be 16, Fig. 8. This was true for all the compositions we investigated in this series. The volume of the $\sqrt{2} \times \sqrt{2} \times 16$ supercell is 32 times the volume of the primitive cubic volume and is considerably less (6.75 times) than the volume of the $6 \times 6 \times 6$ cubic supercell. We therefore considered $\sqrt{2} \times \sqrt{2} \times 16$ as the most probable modulation in the nonpolar phase of our system. A structural model was sought in the orthorhombic space group *Pbnm* for this modulation cell type. The Rietveld fitted NPD of 0.01 KNN is shown in Fig. 9, and the refined structural parameters are given in Table I. The large displacement parameters of the A-site cations may suggest that the long-period modulated structure is accompanied by a significant static disorder of the A-site cations. The large value of the thermal displacement parameters can also arise due to the fact that for a given Wyckoff position, the different A-site cations Na, Bi, K, and Ba were constrained to have same fractional coordinates and thermal displacement parameters during the structural refinement. As shown in the insets of Fig. 9, this single phase model could account for the superlattice reflections reasonably well, confirming the correctness of our approach. Based on the x, y positions of the oxygen atoms, we show in Fig. 10 the complex tilt configuration along the long-period modulation direction of this system.

D. Field-induced structural transformation

The XRPD pattern of the poled specimens of $x = 0.01$ shows [Fig. 5(a)] new peaks flanking the fundamental cubic peaks. The NPD pattern of the poled specimen shows enhanced intensity at the $\frac{1}{2}\{ooo\}_c$ superlatice peak positions, characteristics of the $R3c$ phase, Fig. 11(a). It is therefore evident that the occurrence of a weak but sharp dielectric anomaly on heating the poled specimen of $x = 0.01$ in Fig. 3(a) is associated with the stabilization of the $R3c$ phase after poling. This was further confirmed by heating the poled specimen just above the sharp dielectric anomaly temperature and noticing the disappearance of the $R3c$ Bragg peaks. The XRPD and NPD of the poled $x = 0.015$, on the other hand, do not show any sign of the $R3c$ phase (Figs. 5 and 11) and is consistent with the absence of a sharp dielectric anomaly for this composition, Fig. 3(c). We also carried out an *in situ* electric-field-dependent XRD measurement on a pellet of $x = 0.01$, Fig. 12. An abrupt splitting of the main Bragg peaks becomes evident at a field of 35 kV/cm. This abrupt structural transformation is consistent with the abrupt increase in the piezostrain above 35 kV/cm for this composition (Fig. 1) and confirms that the giant piezostrain is due to the sudden transformation of the long-period modulated structure to the $R3c$ phase above this critical field.

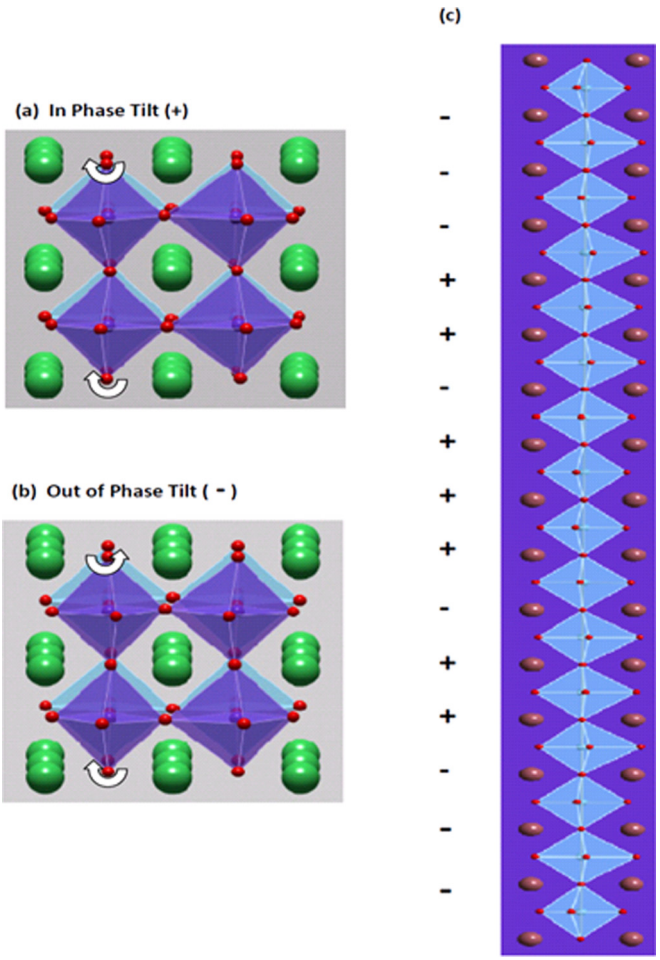

FIG. 10. Schematic of relative rotation of the neighboring octahedra along a vertical tilt axis in a perovskite. (a) shows an in-phase (+) tilt in which the neighboring octahedra are rotated in the same sense about the vertical axis. (b) shows an out-of-phase (−) tilt about the same axis where the neighboring octahedra are rotated in the opposite sense. (c) shows the tilt configuration in the 16× modulated supercell. The tilt relationships between neighboring octahedra in this supercell are specified by the + and − signs.

IV. DISCUSSION

A. Long-period modulation and ferroelectrcity

Since the XRPD patterns of the unpoled specimens do not show superlattice peaks, whereas the neutron powder diffraction patterns do, the superlattice reflections in the NPD owe their origin primarily to subtle displacements of the oxygen atoms from their ideal cubic positions. The distortions corresponding to the two basic octahedral tilts in perovskite, namely, the in-phase (+) tilt and the out-of-phase (−) tilt, shown in Fig. 10, are associated with the R_4^+ and M_3^+ irreducible representations of the cubic ($Pm\text{-}3m$) structure [58]. Vakhrushev and co-workers [59,60] have earlier reported the coexistence of structures with + tilt and − tilts over a wide

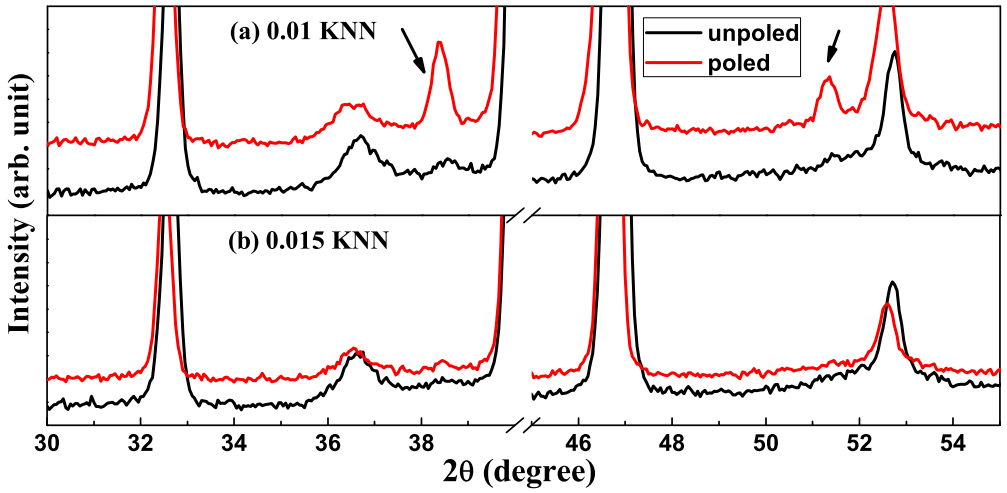

FIG. 11. Neutron powder diffraction patterns of poled and unpoled NBT-BT-KNN for (a) $x = 0.01$ (top panel) and (b) $x = 0.015$ (bottom panel). Arrows indicate intensity enhancement of superlattice peaks, characteristic of the rhombohedral ($R3c$) phase in poled $x = 0.01$.

range of temperatures in NBT. A possibility of competing tilt interactions leading to modulated phases has been suggested and reported by Balagurov *et al.* [18]. Using neutron diffuse scattering the authors reported a long-period modulation in the z direction of the tetragonal ($P4bm$) phase. On cooling, even while the superlative peaks corresponding to the $P4bm$ phase become nonvisible in the diffraction pattern (e.g., at 300 K), the long-period modulation gets locked in the rhombohedral phase [17]. Support in favor of the long-period modulation in NBT came from a high-resolution reciprocal lattice mapping study by Thomas *et al.* [61]. In contrast to the previous diffuse x-ray scattering study by Kreisel *et al.* [15], Thomas *et al.* [61] reported peaking of intensity within the extended diffuse scattering region. The occurrence of the "satellite peaks" reinforces the view that long-period modulation does exist and is perhaps an intrinsic feature of the parent compound (NBT). Chemical modification is likely to affect the nature and the correlation length of this modulation as well as the polar properties. In the present case, it is apparent that the spatial coherence length of the long-period modulation is significantly increased (as compared to that in pure NBT) to enable the characteristic superlattice reflections to become visible in the neutron-diffraction patterns. Concomitantly, the average monoclinic distortion of the NBT lattice transforms to

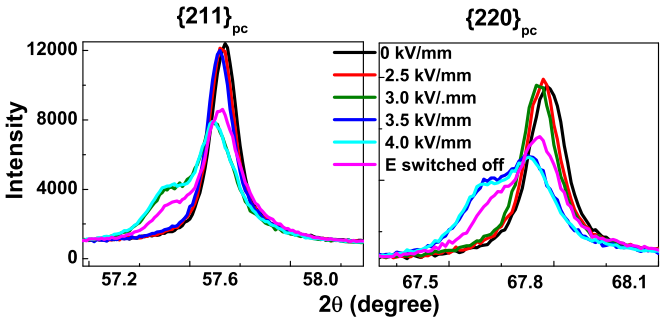

FIG. 12. Evolution of XRD Bragg profiles of $x = 0.01$ as a function of the electric field.

cubiclike. This description of the structure of the nonpolar phase is qualitatively distinct from the $P4bm + R3c$ two-phase models reported before [42].

Long-period modulations of the $\sqrt{2} \times \sqrt{2} \times n$ type have earlier been reported in $NaNbO_3$ [56,62,63], (Sr,Ca)TiO_3 [54], $AgNbO_3$ [64], and $BiFeO_3$ [57]. For $NaNbO_3$ $n = 4$ in the P phase (300–650 K), $n = 6$ in the R phase (650–770 K), and $n = 12$ in the S phase (755–825 K). The modulated phases reported in (Sr,Ca)TiO_3 and $AgNbO_3$ correspond to $n = 4$. For $BiFeO_3$ n has been predicted to be 4 and 6, although the authors have indicated that the system may adopt any other modulation because of the small energy difference between the different modulated phases. In the present system $n = 16$. Following Howard *et al.* [65] the primary distortion corresponding to the $\sqrt{2} \times \sqrt{2} \times n$ modulation can be associated with a point $k = [1/2,1/2,\xi]$ with $\xi = 1/n$ on the T line of symmetry in the first Brillouin zone of the primitive cubic cell. From the tilt configuration corresponding to $n = 16$ of our system, shown in Fig. 10, it is evident that this long-period modulation is composed of both local in-phase (+) and out-of-phase (−) octahedral tilts. The long-period modulation, therefore appears to incorporate both the tilt tendencies [in phase (+) as well as out of phase (−)] inherent in this system. This may be the system's way to minimize its energy by avoiding the formation of interphase boundaries and domains, a situation which could not be avoided had the system settled in a $R3c + P4bm$ phase coexistence. An important question that needs to be addressed is how the different tilt configurations collaborate/compete with the ordering of electric dipoles in the system. Bellaiche and Íñiguez [66] have argued about a universal collaborative coupling between octahedral tilt and antiferroelectric distortions in perovskites. In this context, it may be emphasized that in situations where the long-period modulations comprise a combination of + and − tilts as in (Sr,Ca)TiO_3 and $NaNbO_3$ ($n = 4$, tilt sequence "+ - +") the antiferroelectric state is stabilized. There is no instance of a long-range ordered ferroelectric phase stabilized in a long-period modulated perovskite structure. It is evident from the works of Rao *et al.* [14], Balagurov *et al.* [18], and Thomas *et al.* [61] that the

presence of long-period modulation makes NBT behave as a relaxer ferroelectric. In view of this, it is not surprising that our system also exhibits a strong relaxor behavior because the significant increase in the spatial coherence of the long-period modulation.

B. Giant piezoelectric response and its decay after poling

Whereas the observation of the $R3c$ phase in the poled specimen of $x = 0.01$ proves that the electric field indeed transforms the long-period modulated structure to the $R3c$ phase, the absence of the $R3c$ phase in the poled specimens of $x = 0.015$ can be interpreted in two ways: (i) the nonpolar to ferroelectric transformation is completely reversible or (ii) the applied field of 50 kV/cm was not sufficient enough to induce the transformation in the first place. The fact that $x = 0.015$ shows considerable strain of 0.20% at 48 kV/cm seems to suggest that the strain achieved is due to field-induced transformation. The ferroelectric $R3c$ phase, however, seems to have disappeared on removal of the field for this composition. One important fact to note is the remarkable difference in the shapes of the strain-field (S-E) curves of $x = 0.01$ and $x = 0.015$. Whereas $x = 0.01$ exhibits an abrupt increase in polarization and strain values in the field range of 35−40 kV/cm, the strain increases smoothly and gradually for $x = 0.015$ (Figs. 1 and 2). Importantly, the curvature of the S-E curve during the increasing field is positive and is negative during the decreasing field for $x = 0.01$. Both curvatures are, on the other hand, positive for $x = 0.015$. The abrupt rise in the strain for $E > 35$ kV/cm in $x = 0.01$ suggests that field-induced phase transition is also abrupt and happens above a threshold field. This is evident from the *in situ* electric-field-dependent diffraction shown in Fig. 12. An abrupt jump in strain has also been reported in single crystals of lead-based morphotropic phase boundary systems [67]. For $x = 0.015$, although the strain value of 0.2% at 48 kV/cm is still large enough to suggest the occurrence of field-induced transformation [68] however, unlike $x = 0.01$, this transformation is gradual in nature up to 50 kV/cm, which was the highest field in our study because of the electric breakdown of the specimens. It may also be possible that the abrupt rise in strain may happen above 50 kV/cm for $x = 0.015$. Kling *et al.* [34] have reported a sudden jump in the strain curve at a field around 70 kV/cm for 0.03 KNN.

Our results suggest that the decrease in the giant strain after the first field cycle and more so after poling is caused by retention of the field-induced $R3c$ phase. Since the giant strain at a relatively lower field (∼35 kV/cm) is due to field-induced transformation of the long-period modulated structure to the $R3c$ phase, the piezostrain that can be achieved in a subsequent cycle would be dependent on the volume fraction of the long-period modulated nonpolar phase. For example, if after the first cycle the α fraction of the transformed phase ($R3c$) is retained, in the next cycle the maximum achievable strain due to field-induced transformation would be limited by the transformation of the remaining $(1 - \alpha)$ volume fraction of the long-period modulated structure to the $R3c$ phase. Evidently this will lead to smaller overall piezostrain in the next cycle. This explains the cause of the electrical fatigue related to the giant piezoresponse in such systems. The depolarization temperature would play a crucial role in determining the extent of the retention of the $R3c$ phase at room temperature. If, for example, the depolarization temperature is significantly above room temperature, the extent of the $R3c$ phase retained at room temperature is likely to be more. Such a system would fatigue relatively faster as compared to the one which has its depolarization temperature very close to the room temperature. Towards the end, we may note that there may be a correlation between the critical field required for obtaining giant piezostrain and the depolarization temperature. The fact that we were unable to pole the system at room temperature when the composition changed slightly from $x = 0.01$ to $x = 0.015$, even after application of 50 kV/cm, seems to indicate that the critical field desired for inducing an abrupt increase in strain increases sharply with decreasing values of depolarization temperature.

V. CONCLUSIONS

A neutron-diffraction study was carried out to investigate the structure of the nonpolar phase and the field-induced phase transformation of the NBT-based lead-free system exhibiting giant piezostrain. We show that the conventional $R3c + P4bm$ two-phase description is inadequate to explain the subtle features in the neutron-diffraction pattern. Our study rather reveals the occurrence of a long-period modulated structure of the type $\sqrt{2} \times \sqrt{2} \times 16$ due to competing antiferrodistortive modes. The giant piezostrain is associated with the field-induced transformation of the long-period modulated structure to a rhombohedral ($R3c$) ferroelectric phase. We also show that if the field-induced $R3c$ phase is partly retained the piezostrain is substantially reduced. A possible correlation among depolarization temperature, fatigue in the piezostrain, and the critical field required to effect a field-induced transformation has also been indicated. The mechanism presented in this paper will help with a better appreciation of structure-property correlations in such classes of materials.

ACKNOWLEDGMENTS

R.R. acknowledges the Science and Engineering Board (SERB) of the Department of Science and Technology, Government of India for financial assistance (Grant No. SERB/F/5046/2013-14).

[1] J. Rödel, W. Jo, K. T. Seifert, E.-M. Anton, T. Granzow, and D. Damjanovic, J. Am. Ceram. Soc. **92**, 1153 (2009).
[2] Y. Saito, H. Takao, T. Tani, T. Nonoyama, K. Takatori, T. Homma, T. Nagaya, and M. Nakamura, Nature (London) **432**, 84 (2004).
[3] W. Liu and X. Ren, Phys. Rev. Lett. **103**, 257602 (2009).
[4] A. K. Kalyani, H. Krishnan, A. Sen, A. Senyshyn, and R. Ranjan, Phys. Rev. B **91**, 024101 (2015).
[5] I. Levin and I. M. Reaney, Adv. Funct. Mater. **22**, 3445 (2012).

[6] B. N. Rao, A. N. Fitch, and R. Ranjan, Phys. Rev. B **87**, 060102 (2013).
[7] R. Beanland and P. A. Thomas, Phys. Rev. B **89**, 174102 (2014).
[8] D. S. Keeble, E. R. Barney, D. A. Keen, M. G. Tucker, J. Kreisel, and P. A. Thomas, Adv. Funct. Mater. **23**, 185 (2013).
[9] W. Jo, J. E. Daniels, J. L. Jones, X. Tan, P. A. Thomas, D. Damjanovic, and J. Rödel, J. Appl. Phys. **109**, 014110 (2011).
[10] R. Garg, B. N. Rao, A. Senyshyn, P. S. R. Krishna, and R. Ranjan, Phys. Rev. B **88**, 014103 (2013).
[11] C. Ma, H. Guo, and X. Tan, Adv. Funct. Mater. **23**, 5261 (2013).
[12] E. Aksel, J. S. Forrester, J. C. Nino, K. Page, D. P. Shoemaker, and J. L. Jones, Phys. Rev. B **87**, 104113 (2013).
[13] S. T. Zhang, A. B. Kounga, E. Aulbach, H. Ehrenberg, and J. Rödel, Appl. Phys. Lett. **91**, 112906 (2007).
[14] B. N. Rao, R. Datta, S. S. Chandrashekaran, D. K. Mishra, V. Sathe, A. Senyshyn, and R. Ranjan, Phys. Rev. B **88**, 224103 (2013).
[15] J. Kreisel, P. Bouvier, B. Dkhil, P. A. Thomas, A. M. Glazer, T. R. Welberry, B. Chaabane, and M. Mezouar, Phys. Rev. B **68**, 014113 (2003).
[16] V. Dorcet and G. Trolliard, Acta Mater. **56**, 1753 (2008).
[17] G. O. Jones and P. A. Thomas, Acta Crystallogr., Sect. B: Struct. Sci., Cryst. Eng. Mater. **58**, 168 (2002).
[18] A. M. Balagurov, E. Y. Koroleva, A. A. Naberezhnov, V. P. Sakhnenko, B. N. Savenko, N. V. Ter-Oganessian, and S. B. Vakhrushev, Phase Transitions **79**, 163 (2006).
[19] S. Gorfman and P. A. Thomas, J. Appl. Crystallogr. **43**, 1409 (2010).
[20] E. Aksel, J. S. Forrester, J. L. Jones, P. A. Thomas, K. Page, and M. R. Suchomel, Appl. Phys. Lett. **98**, 152901 (2011).
[21] B. N. Rao and R. Ranjan, Phys. Rev. B **86**, 134103 (2012).
[22] B. N. Rao, L. Olivi, V. Sathe, and R. Ranjan, Phys. Rev. B **93**, 024106 (2016).
[23] C. Ma, H. Guo, S. P. Beckman, and X. Tan, Phys. Rev. Lett. **109**, 107602 (2012).
[24] B. N. Rao, D. K. Khatua, R. Garg, A. Senyshyn, and R. Ranjan, Phys. Rev. B **91**, 214116 (2015).
[25] R. Ranjan and A. Dviwedi, Solid State Commun. **135**, 394 (2005).
[26] S. T. Zhang, A. B. Kounga, E. Aulbach, T. Granzow, W. Jo, H. J. Kleebe, and J. Rödel, J. Appl. Phys. **103**, 034107 (2008).
[27] R. A. Malik, J. Kang, A. Hussain, C. W. Ahn, H. S. Han, and J. S. Lee, Appl. Phys. Express **7**, 061502 (2014).
[28] R. Cheng, C.Wang, Z. Xu, R. Chu, J. Hao, H. Li, W. Li, J. Dua, and G. Li, RSC Adv. **5**, 90508 (2015).
[29] R. Cheng, Z. Xu, R. Chu, J. Hao, J. Du, and G. Li, J. Eur. Ceram. Soc. **36**, 489 (2016).
[30] S. T. Zhang, A. B. Kounga, E. Aulbach, W. Jo, T. Granzow, H. Ehrenberg, and J. Rödel, J. Appl. Phys. **103**, 034108 (2008).
[31] W. Jo, T. Granzow, E. Aulbach, J. Rödel, and D. Damjanovic, J. Appl. Phys. **105**, 094102 (2009).
[32] X. Tan, E. Aulbach, W. Jo, T. Granzow, J. Kling, M. Marsilius, H. J. Kleebe, and J. Rödel, J. Appl. Phys. **106**, 044107 (2009).
[33] S. T. Zhang, L. Wang, Y. F. Chen, and A. B. Kounga, J. Am. Ceram. Soc. **93**, 1561 (2010).
[34] J. Kling, X. Tan, W. Jo, H. J. Kleebe, H. Fuess, and J. Rödel, J. Am. Ceram. Soc. **93**, 2452 (2010).
[35] M. Hinterstein, M. Knapp, M. Hölzel, W. Jo, A. Cervellino, H. Ehrenberg, and H. Fuess, J. Appl. Crystallogr. **43**, 1314 (2010).
[36] H. Y. Ma, X. M. Chen, J. Wang, K. T. Huo, H. L. Lian, and P. Liu, Ceram. Int. **39**, 3721 (2013).
[37] C. M. Fancher, T. Iamsasri, J. E. Blendell, and K. J. Bowman, Mater. Res. Lett. **1**, 156 (2013).
[38] J. Hao, C. Ye, B. Shen, and J. Zhai, J. Appl. Phys. **114**, 054101 (2013).
[39] J. Kling, W. Jo, R. Dittmer, S. Schaab, and H. J. Kleebe, J. Am. Ceram. Soc. **96**, 3312 (2013).
[40] C. Groh, W. Jo, and J. Rödel, J. Am. Ceram. Soc. **97**, 1465 (2014).
[41] E. Sapper, A. Gassmann, L. Gjødvad, W. Jo, T. Granzow, and J. Rödel, J. Eur. Ceram. Soc. **34**, 653 (2014).
[42] L. A. Schmitt, M. Hinterstein, H. J. Kleebe, and H. Fuess, J. Appl. Crystallogr. **43**, 805 (2010).
[43] F. Fu, J. Zhai, Z. Xu, W. Bai, and X. Yao, Solid State Sci. **13**, 934 (2011).
[44] R. Dittmer, W. Jo, J. Rödel, S. Kalinin, and N. Balke, Adv. Funct. Mater. **22**, 4208 (2012).
[45] W. Jo, E. Erdem, R. A. Eichel, J. Glaum, T. Granzow, D. Damjanovic, and J. Rödel, J. Appl. Phys. **108**, 014110 (2010).
[46] S. Gupta and S. Priya, Appl. Phys. Lett. **102**, 012906 (2013).
[47] C. Groh, W. Jo, and J. Rödel, J. Appl. Phys. **115**, 234107 (2014).
[48] X. Liu and X. Tan, Adv. Mater. **28**, 574 (2016).
[49] D. Maurya, Y. Zhou, Y. Wang, Y. Yan, J. Li, D. Vieland, and S. Priya, Sci. Rep. **5**, 8595 (2015).
[50] J. Rodrigues-Carvajal, *FULLPROF. A Rietveld Refinement and Pattern Matching Analysis Program* (Laboratoire Leon Brillouin, CEA-CNRS, France, 2000).
[51] Z. Luo, T. Granzow, J. Glaum, W. Jo, J. Rödel, and M. Hoffman, J. Am. Ceram. Soc. **94**, 3927 (2011).
[52] A. Le Bail, H. Duroy, and J. L. Fourquet, Mater. Res. Bull. **23**, 447 (1988).
[53] A. M. Glazer, Acta Crystallogr., Sect. B: Struct. Sci.,Cryst. Eng. Mater. **28**, 3384 (1972).
[54] R. Ranjan, D. Pandey, and N. P. Lalla, Phys. Rev. Lett. **84**, 3726 (2000).
[55] R. Ouillon, J. P. P. Lucarre, P. Ranson, P. Pruzan, S. K. Mishra, R. Ranjan, and D. Pandey, J. Phys.: Condens. Matter **14**, 2079 (2002).
[56] S. K. Mishra, R. Mittal, V. Y. Pomjakushin, and S. L. Chaplot, Phys. Rev. B **83**, 134105 (2011).
[57] S. Prosandeev, D. Wang, W. Ren, J. Iniguez, and L. Bellaiche, Adv. Funct. Mater. **23**, 234 (2013).
[58] C. J. Howard and H. T. Stokes, Acta Crystallogr., Sect. B: Struct. Sci., Cryst. Eng. Mater. **54**, 782 (1998).
[59] S. B. Vakhrushev, V. A. Isupov, B. E. Kvyatkovsky, N. M. Okuneva, I. P. Pronin, G. A. Smolensky, and P. P. Syrnikov, Ferroelectrics **63**, 153 (1985).
[60] S. B. Vakhrushev, S. B. Vakhrushev, R. S. Malysheva, N. M. Okuneva, E. L. Plachenova, and P. P. Syrnikov, Kristallografiya **34**, 154 (1989).
[61] P. A. Thomas, S. Trujillo, M. Boudard, S. Gorfman, and J. Kreisel, Solid State Sci. **12**, 311 (2010).
[62] C. N. W. Darlington and K. S. Knight, Physica B **266**, 368 (1999).
[63] M. D. Peel, S. P. Thompson, A. Daoud-Aladine, S. E. Ashbrook, and S. E. Lightfoot, Inorg. Chem. **51**, 6876 (2012).

[64] M. Yashima, S. Matsuyama, R. Sano, M. Itoh, K. Tsuda, and D. Fu, Chem. Mater. **23**, 1643 (2011).
[65] C. J. Howard, R. L. Withers, K. S. Knight, and Z. Zhang, J. Phys.: Condens. Matter **20**, 135202 (2008).
[66] L. Bellaiche and J. Íñiguez, Phys. Rev. B **88**, 014104 (2013).
[67] M. Davis, D. Damjanovic, and N. Setter, Phys. Rev. B **73**, 014115 (2006).
[68] M. Hinterstein, M. Hoelzel, J. Rouquette, J. Haines, J. Glaum, H. Kungl, and M. Hoffman, Acta Mater. **94**, 319 (2015).